Conformations, Interactions, and Thermostabilities of RNA and Proteins in Bean Pod Mottle Virus: Investigation of Solution and Crystal Structures by Laser Raman Spectroscopy†

Tiansheng Li,‡ Zhongguo Chen,§ John E. Johnson,§ and George J. Thomas, Jr.*,‡

Division of Cell Biology and Biophysics, School of Biological Sciences, University of Missouri—Kansas City, Kansas City, Missouri 64110, and Department of Biological Sciences, Purdue University, West Lafayette, Indiana 47907

Received February 13, 1992; Revised Manuscript Received April 22, 1992

ABSTRACT: We report and interpret laser Raman spectra of the three virion components of bean pod mottle virus (BPMV). The top component of BPMV is an empty capsid; middle and bottom components package the RNA2 and RNA1 genome segments, respectively. All components were investigated as both single *crystals* and aqueous *solutions*, the latter over wide ranges of temperature and ionic strength. The isolated RNA2 molecule of BPMV middle component was also investigated in both H_2O and D_2O solutions. The results permit assessment of RNA and protein structures, their mutual interactions in the virions, and their conformational thermostabilities and comparison of these structural characteristics for solution and crystal states of the particles. The principal findings of this study are (i) The extent of ordered A-form backbone (74%) and of base pairing (38% AU + 22% GC) in unpackaged (aqueous) RNA2 are significantly altered by packaging. The A-form secondary structure of RNA2 is increased by 12 ± 4%, and guanine base interactions are also substantially increased with packaging. (ii) The thermostability of Raman-monitored secondary structure of unpackaged RNA2 ($T_m \approx 43$ °C) is greatly increased in the packaged state ($T_m \approx 53$ °C). This increase corresponds to a stabilization of the A-form backbone geometry in 15 ± 5% of genome nucleotides. (iii) Packaging of RNA2 in the middle component stabilizes subunit–subunit interactions of the capsid, as evidenced by a thermal denaturation temperature $T_d \approx 65$ °C for the virion, compared with $T_d \approx 55$ °C for the empty capsid. (iv) Raman marker-band shifts implicate the purine 7N sites of RNA2 and aromatic side chains of subunits as the principal targets for RNA–subunit interaction. (v) At the conditions of the present experiments (8 °C, pH ≈ 7, moderate ionic strength), the subunit secondary structures observed for solutions of the top, middle, and bottom components are indistinguishable by Raman spectroscopy from secondary structures observed for corresponding crystalline samples. (vi) On the other hand, side chains of subunits in the top component (empty capsid) yield significantly different Raman intensities in crystalline and solution states. These differences are interpreted as the result of changes in a small number of side-chain environments between crystal and solution. (vii) Similarly, small differences exist between RNA Raman markers of crystalline and aqueous virions, which are attributed to altered environments of nucleotide residues and to a small increase in the amount of A-form backbone geometry upon going from the crystal to the solution. (viii) We have compared the Raman spectral differences between crystal and solution states of BPMV components with spectral differences observed as a function of solution ionic strength. The results lead to the conclusion that Raman spectral differences between crystal and solution forms of the virions are mainly the consequence of different electrostatic environments of the packaged RNA molecules in the two states.

Bean pod mottle virus (BPMV) is a member of the plant comovirus family. Its genome consists of two positive-sense single-stranded RNA (ssRNA) molecules, RNA1 (2.5×10^6 Da) and RNA2 (2.0×10^6 Da), packaged respectively in bottom and middle virion components. RNA1 codes for proteins involved in viral replication and RNA2 for coat and assembly proteins. Both RNA1 and RNA2 are required for infection, and both are translated as polyproteins that are subsequently processed by viral encoded proteases. The 3′ terminus of each RNA is polyadenylated, and the 5′ terminus is covalently linked to a small protein (VPg). The empty capsid (top component), which constitutes about one-fifth of particles formed in vivo, consists of 60 copies each of a large (42-kDa) and small (24-kDa) subunit. The capsids of top, middle, and bottom components form isomorphous crystals and are structurally identical, except for changes in the N-terminal 18 residues of the large protein subunit. These residues are internal and their electron densities are weak or nonexistent in the empty capsid, suggesting greater mobility for these residues in the empty capsid compared with the nucleoprotein components (Johnson et al., 1989; Lomonossoff & Johnson, 1991).

The 3.0-Å crystal structure of BPMV middle component shows that the two proteins of the capsid form three β-barrels organized on a $T = 3$ lattice (Chen et al., 1989). The subunit design is consistent with protein folds in capsids of other icosahedral plant, animal, and bacterial viruses (Lomonossoff & Johnson, 1991). The electron density map also reveals features at the three-fold vertices of the capsid which are assignable to ordered domains of the packaged RNA2 molecule, accounting for approximately 20% of the nucleotide residues. Significant regions of ordered DNA have also been observed

† This is Part XXXV in the series Studies of Virus Structure by Laser Raman Spectroscopy, supported by National Institutes of Health Grants AI11855 (G.J.T.) and AI18764 (J.E.J.).

* Author to whom correspondence should be addressed.
‡ University of Missouri—Kansas City.
§ Purdue University.

0006-2960/92/0431-6673$03.00/0

in crystal structures of canine parvovirus (Tsao et al., 1991) and bacteriophage ϕX174 (McKenna et al., 1992). The BPMV crystal structure indicates that the ordered RNA nucleotides form contacts with hydrophilic side chains and maintain a backbone stereochemistry approximating one strand of A-type RNA (Chen et al., 1989). However, the map does not indicate whether the ordered single-stranded domain forms additional contacts with other RNA segments, protein groups, or solvent that lack icosahedral symmetry.

The remaining 80% of the packaged RNA2 molecule is not revealed in the 3.0-Å crystal structure. Its conformation and putative interactions with capsid protein are not known. We have employed Raman spectroscopy to further investigate the conformations of RNA and protein constituents of BPMV, in solution and in the crystal. Our objectives include determination of (i) the extent of A-form secondary structure in the backbone of BPMV RNA in packaged and unpackaged states, (ii) the extent of formation of AU and GC base pairs in BPMV RNA, (iii) the thermostabilities of RNA secondary structures in packaged and unpackaged states, (iv) the thermostabilities of subunit secondary structures in virions and empty capsids, and (v) the nature and extent of RNA–protein interactions in virions of aqueous and crystalline states.

Previously, we employed Raman spectroscopy to investigate structures of BPMV top, middle, and bottom components in aqueous solution at a single temperature (8 °C) and to compare the solution and crystal structures of BPMV middle component (Li et al., 1990). The earlier results indicated that the subunit secondary structure of the middle component was unchanged and that the structure of packaged RNA2 was also largely conserved between crystal and solution. However, small but significant spectral differences were detected between crystal and solution, and these were assigned to minor changes in molecular environment of the packaged RNA2 at these experimental conditions. Here, we extend the comparative analysis of crystal and solution structures to the BPMV bottom and top components over a wider range of experimental conditions. We have examined Raman spectra of BPMV as a function of salt concentration in order to determine the dependence of the Raman signature upon effective ionic strength and to reach structural conclusions from the data. Dependence of the virion spectrum upon salt concentration would suggest a significant role for electrostatic interactions in determining virion structure and could be related to previously observed differences between crystal and solution spectra (Li et al., 1990).

EXPERIMENTAL PROCEDURES

(I) Isolation and Purification of BPMV

BPMV was isolated and purified using described procedures (Semancik & Bancroft, 1965). The purified virus pellet was centrifuged at 39000 rpm for 18 h in a 4% CsCl gradient to separate four bands corresponding to top (T), middle (M), bottom-upper (B_U), and bottom-lower (B_L) components. The four components were collected and, on the basis of their respective absorption coefficients [$\epsilon_{280} \times 10^3 = 1.2$ (T); $\epsilon_{260} \times 10^3 = 8.1$ (M), 10.0 (B_U), 10.0 (B_L); and $A_{260}/A_{280} = 0.70$ (T), 1.73 (M), 1.79 (B_U), 1.79 (B_L)], were diluted to 10 mg/mL in a buffer containing 0.1 M potassium phosphate plus 10 mM EDTA at pH 7. Each solution was centrifuged at 42000 rpm for 4 h to yield a pellet that was resuspended in the phosphate–EDTA buffer to a final concentration of 10 mg/mL. RNA2 was isolated from the middle component, purified by phenol extraction, and stored as described (MacFarlane et al., 1991).

(II) Sample Handling for Raman Spectroscopy

An aliquot (150 μL) of the virus or capsid solution was centrifuged at 35000 rpm for 3 h in a Beckman airfuge, and the pellet was resuspended in the appropriate volume of buffer to a final concentration of 100 μg/μL. Approximately 10 μL of this solution was sealed in a glass capillary cell (Kimax 34507) for spectral analysis. RNA2 was dissolved to 50 mg/mL in autoclaved H_2O that had been previously treated with 0.1% diethyl pyrocarbonate. All solution samples were thermostated (to ±0.5 °C) at the specified temperatures while Raman spectra were collected (Thomas & Barylski, 1970). Single crystals of BPMV top, middle, and bottom components (Chen et al., 1989) were sealed in glass capillaries containing the mother liquor and thermostated at 8.0 ± 0.5 °C during data collection.

Spectra collected as a function of temperature (0–70 °C) were obtained from phosphate-free solutions (0.1 M KCl, 10 mM Tris-HCl, pH 7.0) in order to circumvent complications from Raman bands of the phosphate anion. At the virus (protein) concentrations employed, the subunits are self-buffering, as evidenced by the measured pH as a function of temperature. For example, the middle component exhibited a measured pH change from 6.97 at 25 °C to 6.78 at 60 °C. The Raman data were collected on a Spex 1877 triple spectrometer interfaced with an EG&G OMA-III intensified diode array detector (Lamba et al., 1990). Typically, the spectral band pass was set at 549 nm, which encompasses the Stokes Raman interval 640–1750 cm^{-1}. Spectra on the OMA-III were averaged from 40 exposures of 30 s each. Additional data were recorded on a Spex Ramalog 1401 scanning spectrometer under the control of an IBM-AT microcomputer. These data were collected at increments of 1 cm^{-1} with spectral slit width of 8 cm^{-1} and integration time of 1.5 s. Ten spectral scans were averaged for the region 400–1800 cm^{-1}. Further details of data collection have been described (Li et al., 1981). All Raman spectra were excited with the 514.5-nm line of a Coherent Innova 70 argon-ion laser, using approximately 100 mW of radiant power at the sample.

(III) Data Analysis

Solvent and scattering background were subtracted from the signal-averaged spectra by difference methods described elsewhere (Verduin et al., 1984). In order to avoid compounding of spectral noise, which occurs in successive subtractions of spectra, the solvent background was not usually subtracted from pairs of spectra used in subsequent subtractions. On the other hand, when nonidentical buffers were employed, such as in the case of the crystalline and solution forms of the BPMV middle component, we subtracted the respective buffers prior to comparing the Raman spectra by difference spectroscopy.

Generally, difference spectra of nucleic acids were normalized to minimize intensity differences in the 1080–1120 cm^{-1} region, since the intensity of the prominent Raman band in this interval (phosphate dioxy stretching, ca. 1100 cm^{-1}) is invariant to changes in molecular environment or RNA secondary structure (Thomas et al., 1971; Tsuboi et al., 1971). For computation of protein difference spectra, intensities were normalized to minimize differences in protein bands which are largely invariant to the applicable changes of state. As shown previously (Li et al., 1990), this can be accomplished by normalization either to the Raman band near 1005 cm^{-1} due to phenylalanine (phenyl ring breathing) or to the band

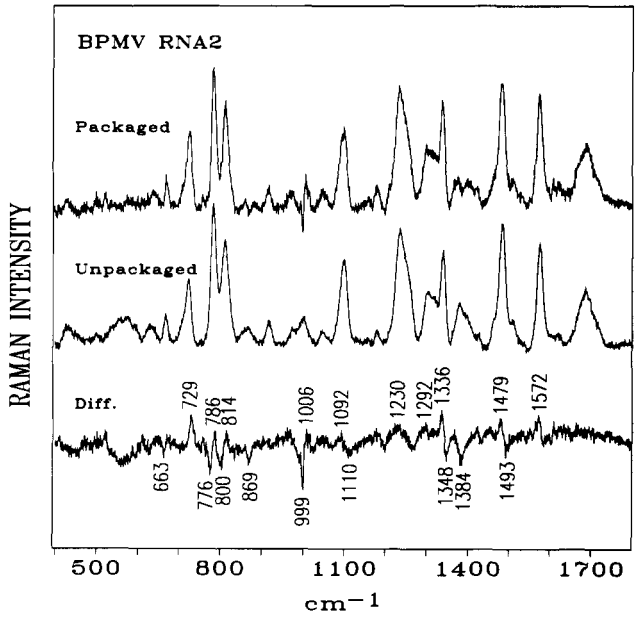

FIGURE 1: (Top): Raman spectrum in the region 400–1800 cm^{-1} of packaged RNA2, from the BPMV middle component in H_2O solution. This spectrum was computed by subtracting the spectrum of the empty capsid (BPMV top component in H_2O solution) from that of the virion. (Middle): Raman spectrum of unpackaged (protein-free) RNA2 in H_2O solution. (Bottom): Raman difference spectrum computed by subtracting the spectrum of unpackaged RNA2 from that of packaged RNA2. All experimental data were recorded from samples prepared in 100 mM KCl + 10 mM Tris at pH 7 and thermostated at 8.0 ± 0.5 °C.

near 1457 cm^{-1} due to side-chain methylene groups (CH_2 scissoring), depending upon the particular system being examined. When apparent intensity differences occurred in any of these reference bands, the normalizations were refined either to minimize the overall spectral differences or to compensate as much as possible the sum of positive and negative difference bands. Further details of spectral subtraction procedures have been described (Verduin et al., 1984; Li et al., 1990). In the difference spectra discussed here, only peaks which are at least twofold more intense than the baseline noise level have been interpreted structurally.

RESULTS

In this section we present signal-averaged Raman spectra of several BPMV components. These data illustrate quantitatively the spectral differences between (i) packaged and unpackaged states of RNA2, (ii) empty and RNA-filled capsids, (iii) native and thermally denatured states of the capsid, RNA, and virion, and (iv) crystal and solution forms of top, middle, and bottom components. We also show the effects of potassium salts (KCl and KH_2PO_4/K_2HPO_4) on Raman spectra of middle component solutions. These results are interpreted in detail in the Discussion section which follows.

Figure 1 compares Raman spectra in the region 400–1800 cm^{-1} of RNA2 in *packaged* and *unpackaged* states. The spectrum of packaged RNA2 was determined by subtracting the spectrum of the top component from that of the middle component. The spectrum of unpackaged RNA2 was obtained directly from phenol-extracted (protein-free) middle component. The difference spectrum computed between these two states of RNA2, with the packaged form as minuend and the unpackaged form as subtrahend, is included in Figure 1. (Similar spectra were obtained for corresponding D_2O solutions of RNA2, capsid, and virion, and are available as supplementary material, see paragraph at end of paper.) In Figure

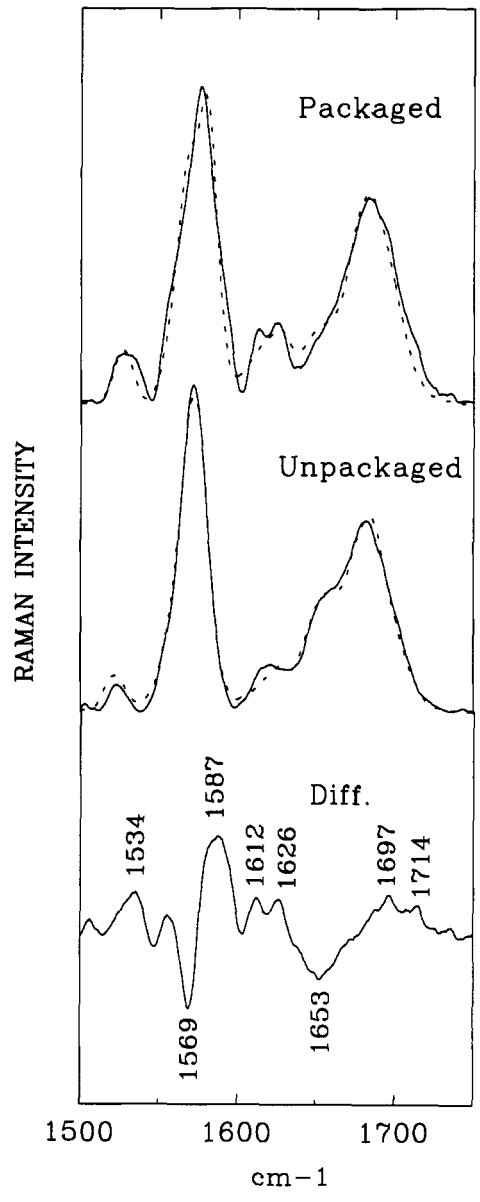

FIGURE 2: (Top): Raman spectrum (—) in the region 1500–1750 cm^{-1} of packaged RNA2, from the BPMV virion in D_2O solution. This spectrum was obtained by subtracting the spectrum of the empty capsid (BPMV top component in D_2O solution) from that of the virion. (Middle): Raman spectrum (—) of unpackaged RNA2 in D_2O solution. Data were obtained from samples prepared in 100 mM KCl + 10 mM Tris at pD 7 and thermostated at 8 °C while spectra were collected. Each experimental spectrum is compared with a synthesized spectrum (– –), obtained by optimal least-squares fit to data from model compounds [phage ϕ6 dsRNA + poly(rA)·poly(rU) + poly(rG)·poly(rC) + rAMP + rUMP + rGMP + rCMP, as described in the text]. The synthesized spectrum of unpackaged RNA2 corresponds to 38% AU and 22% GC, which is consistent with the base composition, while that of packaged RNA2 corresponds to 30% AU and 55% GC, which is inconsistent with the base composition. (See discussion in text.) (Bottom): Raman difference spectrum computed by subtracting the spectrum of unpackaged RNA2 (middle) from that of packaged RNA2 (top).

2 we show the 1500–1750 cm^{-1} interval ("double-bond region") of D_2O solution spectra of packaged and unpackaged RNA2 and the corresponding difference spectrum. The Raman bands of this interval are sensitive to both hydrogen-bonding and stacking interactions of the bases (Thomas, 1969; Morikawa et al., 1975). Each experimental spectrum of Figure 2 is also fitted to a linear combination of spectra obtained from secondary structure models.

Figure 3 compares Raman spectra of unpackaged RNA2

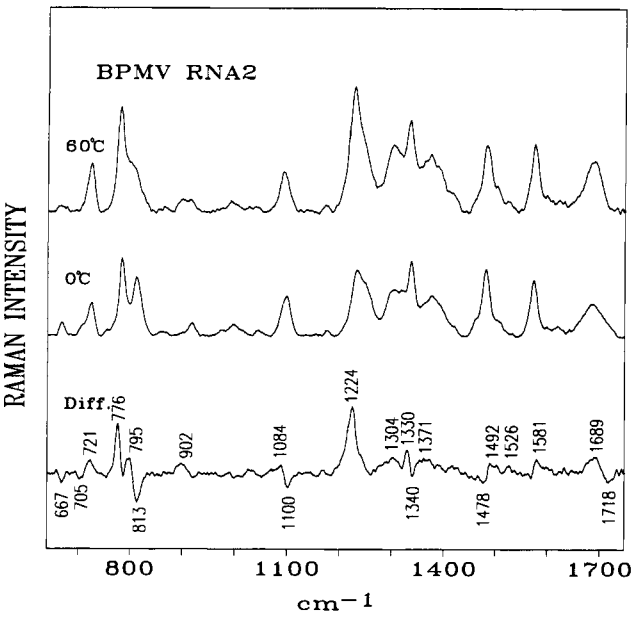

FIGURE 3: (From top to bottom): Raman spectra of unpackaged RNA2 at 60 and 0 °C and their computed difference spectrum (60 minus 0 °C). RNA2 was dissolved to 50 mg/mL in 100 mM KCl + 10 mM Tris at pH 7.

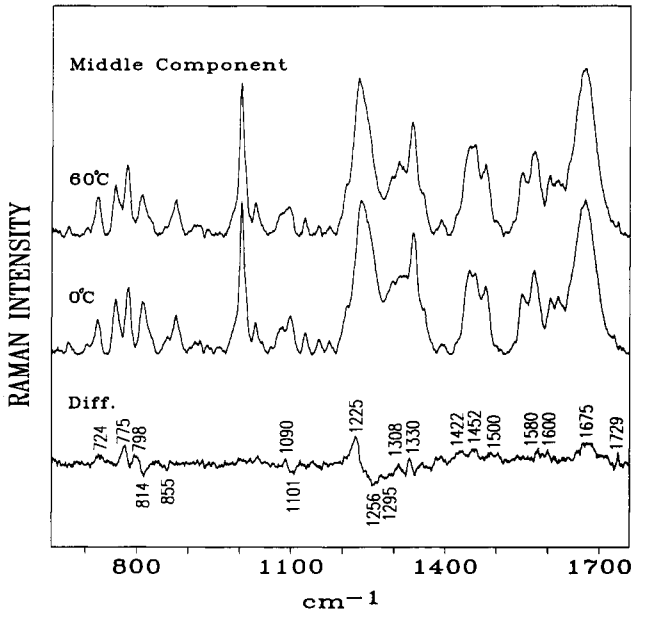

FIGURE 4: (From top to bottom): Raman spectra of BPMV middle component at 60 and 0 °C and their computed difference spectrum (60 minus 0 °C). The virus was dissolved to 100 mg/mL in 100 mM KCl + 10 mM Tris at pH 7.

in solution at 0 and 60 °C. Figure 4 compares spectra of the middle component in solution at 0 and 60 °C. In each case, the solution remains homogeneous at the high temperature. The difference spectra of Figures 3 and 4 largely reflect *RNA2 thermostabilities* for unpackaged and packaged states, respectively. Figure 5 shows Raman melting profiles of RNA2 determined from data of Figures 3 and 4, as well as from additional data (available as supplementary material), which were collected at intervals of 5 °C. We also compared *subunit thermostabilities* in empty and RNA-filled capsids. Figure 6 shows Raman spectra of the top component at 8 and 60 °C. At the former temperature, the capsid is intact and the solution is homogeneous; at the latter temperature, the sample formed a precipitate from which the spectrum was recorded. Comovirus capsid subunits generally are dissociated above 55 °C (Virudachalam et al., 1985). Figure 7 compares spectra of the middle component at 0 and 70 °C. Again, at the lower temperature the solution is homogeneous; at the higher temperature, the sample formed a precipitate from which the spectrum was recorded. Our studies consistently showed that at pH 7 the BPMV virion was more thermostable than the empty capsid, as evidenced by the fact that the middle component resisted precipitation up to 65 °C, while the top component precipitated at ca. 55 °C.

Figure 8 compares Raman difference spectra (crystal minus solution) of BPMV top, middle, and bottom components. These data confirm previously reported differences for *crystal vs solution* states of the middle component (Li et al., 1990) and extend the analysis to the bottom component as well as to empty capsids. Figure 9 shows difference spectra which reflect changes in the solution Raman spectrum of the middle component as the *salt composition* is altered. For each difference spectrum of Figure 9, the minuend was recorded from virus dissolved in the indicated salt solution at pH 7, and the subtrahend was recorded from virus dissolved in pure H_2O (no salt added, but solution pH adjusted to 7 with dilute NaOH).

Additional Raman spectra of BPMV components and of model compounds required for structure analysis or interpretation are available as supplementary material. These include (i) D_2O solution spectra (400–1800 cm^{-1}) of packaged and unpackaged RNA2; (ii) D_2O solution spectra (1500–1750 cm^{-1}) of double-stranded RNA from bacteriophage ϕ6, poly(rA)·poly(rU), poly(rG)·poly(rC), rAMP, rUMP, rGMP, and rCMP; (iii) H_2O solution spectra (650–1750 cm^{-1}) of RNA2 as a function of temperature (0–90 °C); (iv) H_2O solution spectra (650–1750 cm^{-1}) of top component as a function of temperature (0–60 °C); and (v) H_2O solution spectra (650–1750 cm^{-1}) of middle component as a function of temperature (0–70 °C).

DISCUSSION

(I) Structural Differences between Packaged and Unpackaged RNA2

The difference spectrum of Figure 1 exhibits peaks at 729 (A), 786 (U,C), 814 (O–P–O), 1006 (F,r), 1092 (PO_2^-), 1230 (U,C), 1292 (A,C), 1336 (A,G), 1479 (G,A) and 1572 (G,A) cm^{-1} and troughs at 663 (G), 776 (U,C), 800 (O–P–O), 869 (O–P–O,r), 999 (F,r), 1110 (PO_2^-), 1348 (A,G), 1384 (G,A), and 1493 (G,A) cm^{-1}. Except for phenylalanine assignments at 1006 and 999 cm^{-1}, all differences are due to residues of RNA2. The large number of RNA difference bands implicates many types of nucleic acid groups, directly or indirectly, in structure changes associated with packaging. The relatively high amplitudes of the most significant difference bands (≈20% of parent band intensities) are indicative of the large-scale nature of these packaging-induced conformational changes. We discuss in turn structure changes of the RNA backbone and base residues.

(A) Conformational Changes Involving the Phosphodiester Groups. The Raman band at 813 ± 1 cm^{-1} is a marker of the A-form backbone of RNA (Thomas et al., 1971; Small & Peticolas, 1971; Lafleur et al., 1972; Erfurth et al., 1972). The Raman intensity is directly proportional to the number of C–O–P–O–C linkages with torsion angles α and ζ corresponding to the gauche$^-$,gauche$^-$ configuration (Thomas & Hartman, 1973; Thomas et al., 1986). The 1100 cm^{-1} band, assigned to PO_2^- symmetric stretching, is essentially invariant to backbone conformational change. The intensity ratio of

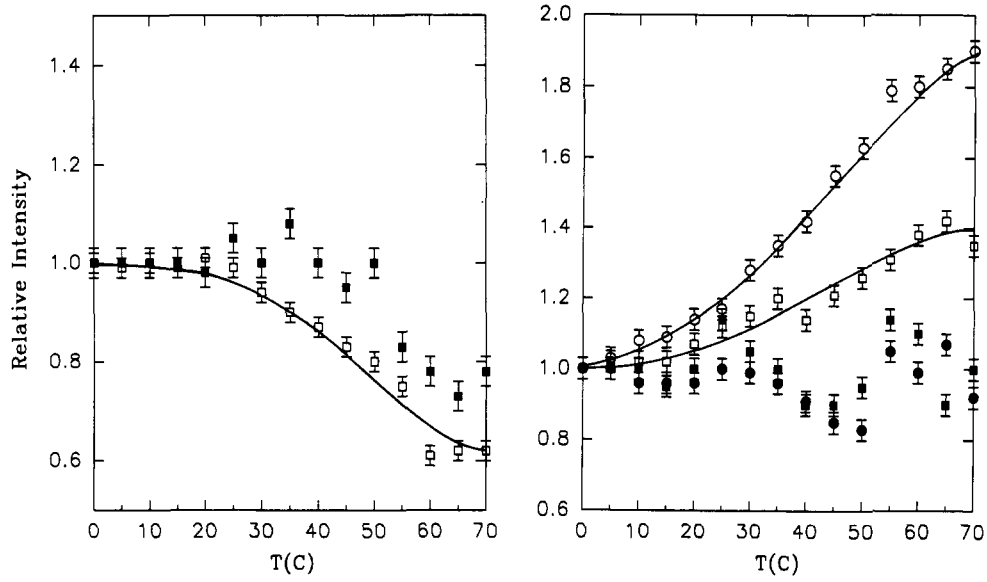

FIGURE 5: (Left): Temperature dependence of Raman intensity ratios I_{813}/I_{1100} of protein-free RNA (□) and I_{813}/I_{1004} of BPMV middle component (■). (Right): Temperature dependence of Raman intensity ratios I_{725}/I_{1100} (□) and I_{1235}/I_{1100} (○) of unpackaged RNA2 and I_{725}/I_{1004} (■) and I_{1235}/I_{1004} (●) of BPMV middle component.

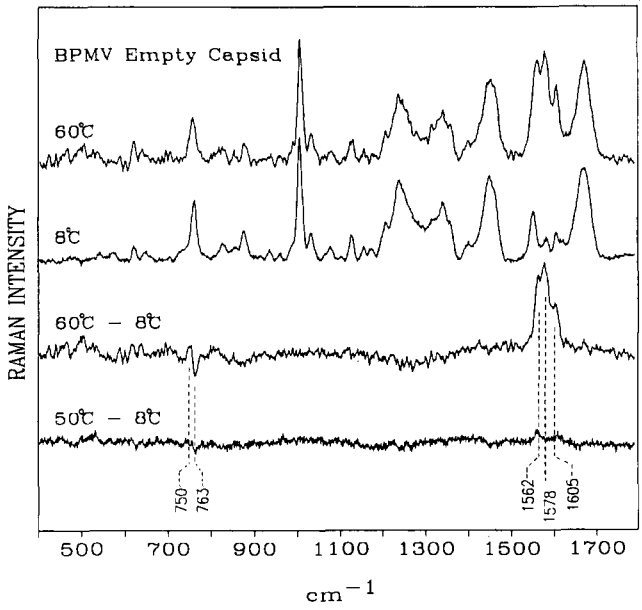

FIGURE 6: (From top to bottom): Raman spectra of the thermally denatured (insoluble) empty capsid at 60 °C, native empty capsid at 8 °C, their difference spectrum (60 minus 8 °C), and a temperature difference spectrum (50 minus 8 °C) between soluble forms. All data were obtained from an initial solution of the capsid at 100 mg/mL in 100 mM M KCl + 10 mM Tris, pH 7.0.

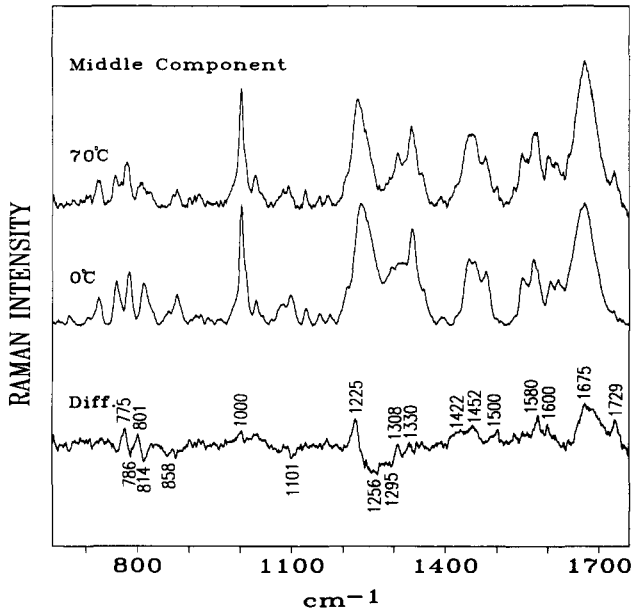

FIGURE 7: (From top to bottom): Raman spectra of the thermally denatured (insoluble) middle component at 70 °C, native middle component at 0 °C, and their difference spectrum (70 minus 0 °C). Data were obtained from an initial solution of the middle component at 100 mg/mL in 100 mM M KCl + 10 mM Tris, pH 7.0.

the 813 and 1100 cm^{-1} bands (I_{813}/I_{1100}) provides a convenient measure of the percentage of ordered A-form backbone geometry in RNA. This ratio achieves a maximum value of 1.64 ± 0.05 in polyribonucleotide duplexes and dsRNA, in which 100% of the backbone assumes the g^-,g^- conformation (Lafleur et al., 1972; Thomas & Hartman, 1973). When the RNA backbone is thermally denatured, the A-form marker band is greatly diminished in intensity and $I_{813}/I_{1100} \approx 0.1$, indicating <10% g^-,g^- conformers.

From the spectra of Figure 1 we find for unpackaged RNA2, $I_{813}/I_{1100} = 1.22 \pm 0.05$ (74 ± 3% ordered backbone) and for packaged RNA2 $I_{813}/I_{1100} \pm 1.41 \pm 0.05$ (86 ± 3% ordered backbone). The difference spectrum of Figure 1 confirms that Raman intensity is shifted from ca. 800 to 814 cm^{-1} with packaging. We interpret this result as evidence that 12 ± 4% of RNA nucleotide residues, which are not regularly ordered in the protein-free RNA2 molecule at the experimental conditions employed here, are converted to the ordered state (A-form backbone) with packaging.

(B) Conformational Changes Involving Ribose and Base Residues. The difference spectrum of Figure 1 exhibits several additional features reflecting structural dissimilarities between nucleosides of packaged and unpackaged RNA2. Although detailed interpretation in terms of specific nucleoside conformational changes is not possible, it is clear that all types of base residues (A, U, G, C) are represented in the difference spectrum. Since the directions of intensity change are not unique, the results cannot be interpreted simply as Raman hypochromic effects associated with changes in base stacking (Small & Peticolas, 1971). The observed difference bands probably result from a combination of intramolecular and environmental changes between packaged and unpackaged

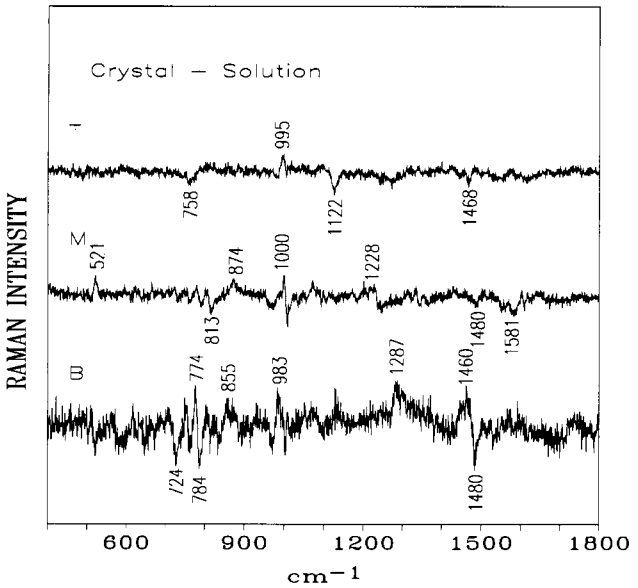

FIGURE 8: Comparison of crystal and solution state Raman spectra in the region 400–1800 cm^{-1} for BPMV top, middle, and bottom components. (Top): Crystal minus solution difference spectrum of the top component. (Middle): Crystal minus solution difference spectrum of the middle component. (Bottom): Crystal minus solution difference spectrum of the bottom component (upper fraction).

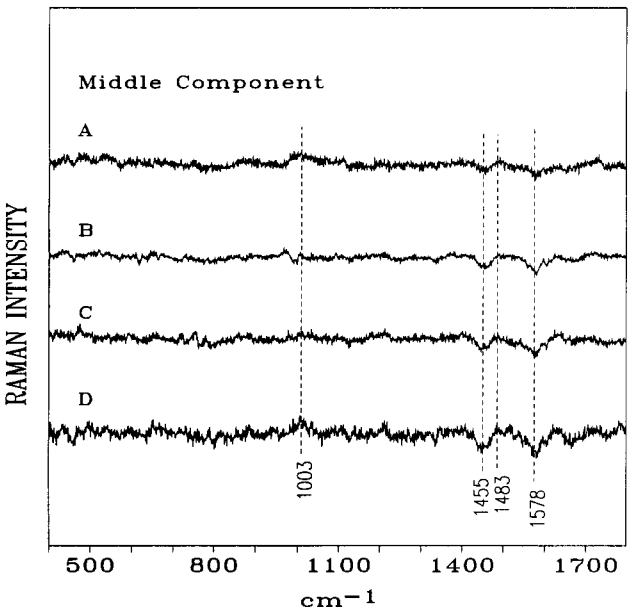

FIGURE 9: Comparison of Raman spectra in the region 400–1800 cm^{-1} of BPMV middle component in solutions containing various potassium salt concentrations. Each difference spectrum (A–D) was obtained by subtracting the Raman spectrum of BPMV middle component in a minimal salt medium (ionic strength ≈ 0.01) from the spectrum obtained at the indicated ionic conditions. (A): BPMV middle component in 0.02 M KH_2PO_4/K_2HPO_4 buffer at pH 7.0. (B): BPMV middle component in 0.1 M KH_2PO_4/K_2HPO_4 buffer at pH 7.0. (C): BPMV middle component in 0.1 M NaCl + 0.01 M KH_2PO_4/K_2HPO_4 buffer at pH 7.0. (D): BPMV middle component in 2.0 M KCl + 10 mM Tris at pH 7.0.

RNA2, involving changes of base stacking, base pairing, major groove interactions, and backbone conformations.

With respect to the shift of intensity from 1493 (unpackaged RNA2) to 1479 cm^{-1} (packaged RNA2), the 7N purine sites are implicated. Nishimura et al. (1986) have demonstrated that this type of intensity shift in guanosine reflects the formation of a specific hydrogen bond to the guanine ring 7N acceptor. The correlation has been confirmed in nucleoprotein complexes containing both A and G residues (Benevides et al., 1991). We conclude that purines of packaged RNA2 are involved in 7N hydrogen-bonding interactions which do not occur for unpackaged RNA2. Hydrogen-bond donation to 7N purine acceptors may originate from donors of the capsid subunits or may result from a specifically folded RNA2 tertiary structure in the virion or from a combination of both of these factors. The magnitude of the observed intensity shift from 1493 to 1479 cm^{-1} represents 13 ± 5% of the total intensity, which suggests a lower limit to the percentage of purines involved. The positive difference band at 729 cm^{-1} (A) together with positive and negative difference bands in the 1300–1400 cm^{-1} interval (A,G) confirm that packaging causes significant changes in molecular environments of the purines. The remaining difference features of Figure 1, particularly in the 750–800 and 1200–1300 cm^{-1} intervals (U,C), implicate also the pyrimidines of RNA2 in the packaging-induced structure changes.

Finally, we note that the negative difference band at 999 and positive difference band at 1006 cm^{-1} are interpreted as a shift of the phenylalanine ring marker with packaging. Clearly, the band cannot be perfectly compensated in the virion by use of the empty capsid (as subtrahend) in the difference computation (Figure 1, legend). These difference features are significant and indicate that environments of subunit phenylalanines are not invariant to RNA packaging.

(C) Differences in Base-Paired Secondary Structure. The difference spectrum of Figure 2 indicates that secondary structures of packaged and unpackaged RNA2 are not identical. Since the parent Raman bands originate largely from carbonyl stretching modes of C, G, and U, they are sensitive to both the hydrogen-bonding states of the C=O groups (Lafleur et al., 1972) and near-neighbor dipole–dipole coupling (Morikawa et al., 1973). Previously, infrared spectra in this interval were employed to determine the extent of RNA base pairs by fitting the observed D_2O solution spectrum to a linear combination of spectra of appropriate models for paired [poly(rA)·poly(rU), poly(rG)·poly(rC)] and unpaired (rAMP, rUMP, rGMP, rCMP) bases (Thomas, 1969). We have extended this approach to the D_2O solution Raman spectrum. However, initial trials with the same basis set did not yield an acceptable fit to the observed RNA2 Raman spectrum. The root mean square deviation (RMSD) of all Raman intensities in the 1500–1750 cm^{-1} interval (251 points) exceeded 5%. We believe that dipole–dipole coupling is the principal source of this discrepancy; i.e., the polyribonucleotide duplexes do not satisfactorily represent typical base-paired domains of RNA2. In order to improve the fit, we included in the basis set the D_2O solution Raman spectrum of double-stranded RNA from bacteriophage $\phi 6$. The mixed-base composition of $\phi 6$ RNA is expected to better represent the effects of dipole coupling in RNA2 hairpins, which do not consist only of polypurine·polypyrimidine sequences.

As shown in Figure 2 (middle), the Raman spectrum observed for unpackaged RNA2 is well approximated (RMSD < 1.9%) by the seven-term linear combination, yielding 22 ± 5% GC pairs, 38 ± 5% AU pairs, 4% unpaired A, 15% unpaired U, 23% unpaired G, and ~2% unpaired C. For packaged RNA2 (Figure 2, top), the carbonyl band profile is strikingly different, as evidenced by the absence of a prominent shoulder ca. 1653 cm^{-1}. A simple interpretation of this result is that packaging of RNA2 greatly alters the hydrogen-bonding states of purine and/or pyrimidine carbonyls. The experimental data for packaged RNA2 cannot be fit satisfactorily to the same basis set employed for unpackaged RNA2.

The larger discrepancy between observed and fitted spectra of packaged RNA2, as compared with unpackaged RNA2, could be due in part to prior spectral subtraction of the protein spectrum from the virion spectrum. However, the more likely explanation for this larger discrepancy is the existence of specific molecular interactions between carbonyl groups of the bases of packaged RNA2 and donor groups of capsid subunits. If significant base–peptide interactions do occur, it seems reasonable that they would not be well modeled by the basis set employed for the curve fitting of Figure 2.

(II) Thermostability of Virion Components

(A) RNA Thermostability in Packaged and Unpackaged States. Figure 3 compares Raman spectra of unpackaged RNA2 at low (0 °C) and high (60 °C) temperatures. Frequencies and assignments of the major difference bands are labeled in the figure. The number of difference bands and their intensities confirm that large-scale changes of secondary and tertiary structures occur for unpackaged RNA2 between 0 and 60 °C. The change in I_{813}/I_{1100} is consistent with disordering of 40 ± 3% of the A-form backbone of unpackaged RNA2 between 0 and 60 °C. Increases of Raman intensities at 721, 776, 902, 1224, 1304, 1330, and 1581 cm^{-1} confirm unstacking of A, U, G, and C residues with increasing temperature (Prescott et al., 1974). The intensity decrease at 667 cm^{-1} indicates fewer C3′-endo/anti conformers of guanosine; and intensity changes of C=O modes in the 1660–1720 cm^{-1} interval reflect melting of base pairs.

A similar comparison of BPMV middle component at low (0 °C) and high (60 °C) temperatures is shown in Figure 4. We note that 60 °C represents a temperature at which the integrity of the virion can be maintained for at least 2 h at the salt concentration employed, as judged by the constancy of the Raman spectrum, its reversibility upon cooling, and the visualization of the virus particles in the electron microscope. Above 70 °C, on the other hand, the virion decomposes rapidly, with attendant irreversible changes in the Raman spectrum and the appearance of a precipitate in the sample cell. The change of I_{813}/I_{1100} determined from Figure 4 shows that only 25 ± 3% of the backbone of packaged RNA2 is disordered between 0 and 60 °C.

Figures 3 and 4 indicate, interestingly, that the structural changes of unpackaged and packaged RNA2 are qualitatively similar but quantitatively different. Several conclusions may be reached from these results. First, since the difference bands of Figure 4 are due exclusively to RNA2, the structure of the capsid subunit is not sufficiently altered to be detected by Raman spectroscopy (<2%). Second, the *nature* of heat-induced structure changes in RNA2 is independent of packaging. Disordering of the phosphodiester backbone, unstacking of bases, and rupture of hydrogen-bonded base pairs are common to both unpackaged and packaged RNA2. Third, the *extent* of thermal perturbation of RNA2 secondary and tertiary structures is, on the other hand, dependent upon packaging. Specifically, we find for packaged RNA2 that the extent of disordering of the backbone with temperature is only about 63% as large as that which occurs in unpackaged RNA2, base unstacking is less than 50% as extensive, and the disruption of C3′-endo/anti conformers of guanosine is roughly one-third as extensive. The shift of Raman intensity from ca. 1475 to ca. 1490 cm^{-1} with increasing temperature, diagnostic of the disruption of nucleotide interactions (purine N7 hydrogen bonding), is only about one-third as large in packaged RNA2 as in unpackaged RNA2. The bands of the 1660–1720 cm^{-1} interval, which are sensitive to base pairing, are also much less altered for packaged RNA2 than for unpackaged RNA2.

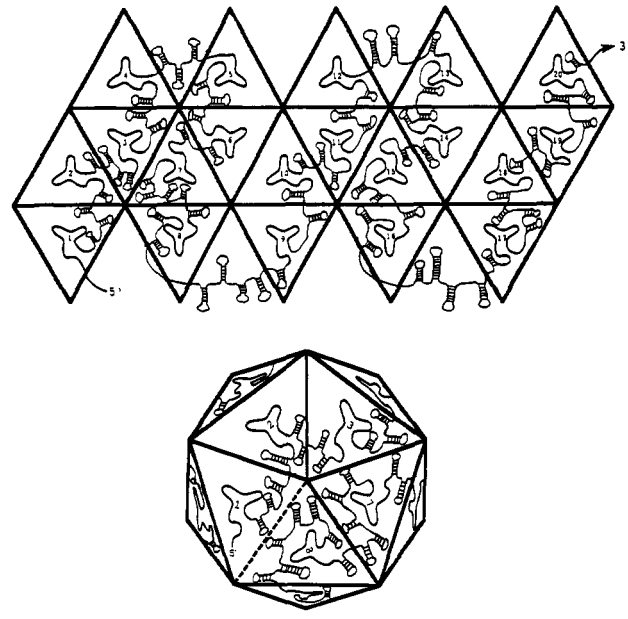

FIGURE 10: Model for RNA packaging that is consistent with Raman and X-ray crystallographic results. (Top): A two-dimensional representation of an icosahedron showing the 20 triangular threefold faces. (Bottom): A view down the fivefold axis of the icosahedron.

Figure 5 compares the temperature dependence of selected Raman band intensities (melting profiles) of RNA2 in unpackaged and packaged states. The midpoint of melting of the A-form backbone, as monitored by the intensity of the 813 cm^{-1} band, is 43 ± 1 °C for unpackaged RNA2 and 53 ± 3 °C for packaged RNA2. These results are interpreted as evidence that approximately 15% of backbone phosphodiester groups are converted from a thermosensitive to a thermostable state by encapsidation, and the T_m of the transition is accordingly shifted by roughly +10 °C. We conclude that the capsid confers considerable thermostability upon the conformation of packaged RNA2, possibly as a result of direct interactions of basic protein groups with RNA phosphates or indirectly through interactions of the RNA bases with subunit residues.

Figure 5 suggests further that median melting temperatures for base–base interactions (stacking) are affected by packaging. We observe, for example, that packaging causes large changes in the melting profiles of the Raman bands at 725 and 1235 cm^{-1}, which are sensitive, respectively, to stacking interactions of A and U. The A and U unstacking transitions display a median temperature of ca. 40 °C in unpackaged RNA2, while comparable transitions are not observed below 60 °C for packaged RNA2 (Figure 5). However, interpretation of these results is not straightforward for the following reason. As the middle component is heated and dissociation of native interactions progresses, these could be supplanted by other RNA–protein interactions, yielding no net change in Raman intensity despite the structural rearrangements.

Figure 10 proposes a model for the packaging of RNA2 which is consistent with the current Raman results and the middle component crystal structure (Chen et al., 1989). This model utilizes the previously proposed RNA trajectory (Lomonossoff & Johnson, 1991). Single-stranded regions of the packaged RNA molecule are threaded through all faces of the icosahedron, maintaining the same polarity about each triad. Since X-ray crystallography identifies nearly 20% of the single-stranded regions of the packaged genome in an

A-type conformation, our data require that the regions of RNA between each triad must contain mainly helical hairpins.

(B) Subunit Thermostability in Empty Capsids and Virions. Figure 6 compares Raman spectra of the native top component with the aggregation product resulting from its thermal denaturation at 60 °C. The Figure 6 difference spectrum reveals dramatic increases in Raman band intensities, particularly at 1562 (Trp), 1578 (Trp, Phe), and 1605 (Phe, Tyr) cm^{-1}, more moderate intensity changes at 750 (Trp) and 763 (Trp) cm^{-1}, and lesser intensity changes in bands assigned to various other side chains (Harada & Takeuchi, 1986; Takeuchi et al., 1991; Li et al., 1990). Since the largest differences occur in bands assigned to Trp, Phe, and Tyr, we conclude that environments of the aromatic side chains, especially indoles, are the most altered by the structure transformation. This transformation presumably involves a combination of capsid disassembly and nonspecific subunit aggregation reactions. Interestingly, the difference spectrum of Figure 6 reveals no net intensity changes in either Raman amide I (1640–1700 cm^{-1}) or amide III (1230–1320 cm^{-1}) bands, indicating little or no net change in subunit secondary structure despite the obviously large changes in quaternary and tertiary structures. This is not surprising considering the high content of β-sheet in the subunit (50–60%) and the relatively high protein concentration employed for the Raman measurements. For example, intramolecular β structure may be replaced by intermolecular β structure. Similar observations have been reported for thermal transformations of the bacteriophage P22 capsid (Prevelige et al., 1990).

As noted above (section IIA and Figure 4), packaging of RNA2 enhances the thermostability of its secondary structure. We observe a reciprocal effect for the capsid subunit. Thus, although the empty capsid disassembles to form protein aggregates at 55 °C (Figure 6), the Raman spectrum of the RNA-filled capsid shows essentially no changes in protein Raman bands up to 60 °C (Figure 4). (Complete Raman spectra at intervals of 5 °C over the range $0 < t < 70$ °C are available as supplementary material.) The virion middle component also remains soluble up to 60 °C, with no visible evidence of protein aggregation until the temperature is increased to 65 °C or higher. Figure 7 compares the middle component Raman spectra at 0 and 70 °C. The difference bands of Figure 7 are distinct, both qualitatively and quantitatively, from those observed for the top component (cf. Figure 6). This is not unexpected, since disassembly of the virion may lead to *ribonucleo*protein aggregates with Raman markers that differ from those of capsid protein aggregates.

(III) Solution and Crystal Structures Compared by Raman Spectroscopy

Figure 8 compares Raman difference spectra, computed as crystal minus solution, for each BPMV component. For the top component (Figure 8, top), there are no amide difference bands and only a few side-chain difference bands of low intensity, indicating that subunit secondary structure is invariant to crystallization and that side chains are minimally affected. The observed difference bands implicate Trp (758), Phe (1000), and aliphatic residues (1122 and 1464 cm^{-1}). No differences are observed in the region 600–900 cm^{-1}, consistent with and confirmatory of conclusions reached previously regarding the effects of crystallization on the BPMV middle component (Li et al., 1990).

For the middle component (Figure 8, middle), the observed differences confirm those reported previously (Li et al., 1990), indicating minor changes in conformations of subunit side chains and packaged RNA2. For the bottom component (Figure 8, bottom), a greater number of difference bands is observed, particularly for the RNA1 molecule. Thus, the difference spectrum between crystal and solution of either virion reveals no change in subunit secondary structure despite changes in subunit side chains and RNA residues. Additionally, we note that the respective difference spectra for middle and bottom components (cf. middle and bottom spectra of Figure 8) reveal no analogy between domains of RNA2 and RNA1 which are structurally sensitive to crystallization. These results are summarized in Table I.

Table I: Assignment and Interpretation of Raman Bands in Difference Spectra between Solutions and Crystals of BPMV Components

frequency (cm^{-1})	top component	middle component	bottom component	ref
521		Ade ring		*a*
724			Ade ring	*b*
758	Trp ring			*c*
784			Cyt,Ura rings	*b*
813		OPO stretch		*b*
855			OPO stretch	*b*
874		OPO stretch		*b*
983			ribose	*b*
1000	Phe ring	Phe ring		*c*
1122	CC stretch			*d*
1228		Tyr ring		*c*
1287			His ring	*c*
1460			CH_2 bend	*c*
			Ade,Gua rings	*b*
1464	CH_2 bend			*c*
1480		Ade,Gua rings	Ade,Gua rings	*b*

[a] Lord and Thomas (1967). [b] Lafleur et al. (1972). [c] Harada and Takeuchi (1986). [d] Lippert and Peticolas (1971).

(IV) Effect of Ionic Strength on BPMV Structure

In order to assess the effects of K^+ and counterions on the Raman spectrum of aqueous BPMV, we recorded data from pH 7 solutions of the middle component, prepared as follows. BPMV was pelleted from a pH 7 virus solution at 10 mg/mL in 0.1 M potassium phosphate + 10 mM EDTA. The pellet was then redissolved in each of the following at pH 7: (i) pure H_2O, (ii) 0.02 M KH_2PO_4/K_2HPO_4, (iii) 0.10 M KH_2PO_4/K_2HPO_4, (iv) 0.1 M NaCl + 0.01 M KH_2PO_4/K_2HPO_4, and (v) 2.0 M KCl + 10 mM Tris.

Figure 9 compares the series of difference spectra obtained by subtracting the spectrum of BPMV in pure H_2O (item i, above) from each spectrum obtained at a higher salt concentration (items ii–v, above). These are labeled A–D, respectively, in Figure 9. Spectral changes from K^+ are confined largely to side-chain bands near 1000 (Phe), 1455 (CH_2), and 1578 cm^{-1} (Trp). Figure 9 shows that these spectral difference bands increase nearly monotonically as the difference in salt concentration increases. Therefore, the salt appears to have an effect upon Raman intensities associated primarily with subunit side chains. Protein and RNA2 secondary structures are apparently unaffected. Although the difference bands of Figure 9 are similar to a few of the features of the middle component difference spectrum (crystal minus solution) of Figure 8, complete correspondence is not observed between the two. We infer that structural changes to the middle component from increasing K^+ activity are not identical to those observed with crystallization, though some similarities are apparent. An obvious dissimilarity between the data of Figure 9 and the middle component data of Figure 8 occurs in the region 600–900 cm^{-1}, where bands assigned

to RNA2 are apparent only in the latter figure.

CONCLUSIONS

The principal conclusions of this study are the following:

The Raman conformation markers of packaged and unpackaged RNA2 indicate major changes of backbone conformation with packaging: 74 ± 3% A-type conformation in unpackaged RNA2 vs 86 ± 3% A form in the packaged state. Regions of A-type conformation (for either unpackaged or packaged RNA) may comprise both base-paired hairpin domains and single-stranded stacked segments, since the Raman markers do not distinguish between the two as long as the phosphodiester torsions α and ζ are in the gauche$^-$/gauche$^-$ range.

Analysis of the D_2O solution Raman spectrum of unpackaged RNA2, by fitting the spectral envelope in the double-bond region to a linear combination of standard spectra representing paired and unpaired structures (seven-state model; data available as supplementary material), indicates 38 ± 5% AU base pairs and 22 ± 5% GC pairs in the unpackaged molecule. The preponderance of AU pairs over GC pairs in unpackaged RNA2 is consistent with the primary base composition (67% A + U, 33% G + C). The inapplicability of the same curve-fitting analysis to packaged RNA2 implies that subunit–nucleotide interactions alter the hydrogen-bonding environments of the base carbonyls.

The increase of A-type backbone conformation induced by RNA packaging—12 ± 4% of the RNA2 molecule—presumably results from specific interactions with capsid subunits. Consistent with this conclusion, we have found that approximately 15% of the A-form backbone structure (813 cm^{-1} band) is thermostabilized by about 10 °C with packaging. We propose that regions of RNA2 which are irregularly configured in the absence of protein achieve an ordered configuration in the capsid as a consequence of specific subunit contacts and that these ordered regions are more thermostable than in the absence of protein. We note that the Raman results are consistent with the percentage (approximate 20%) of ordered ribonucleotides projected from the X-ray diffraction studies. A model for the packaged RNA2 molecule, consistent with both the present Raman results and the previous X-ray structure (Chen et al., 1989) is shown in Figure 10. In this cartoon, which is a refinement of the initial proposal of Lomonossoff and Johnson (1991), we assign single-stranded stacked segments to the 20 trefoils at the icosahedral threefold axes in accordance with the X-ray difference electron density map. This necessitates that the interconnecting, icosahedrally disordered, segments contain virtually all of the base-paired domains (representing 60% or more of all RNA nucleotides), as shown in Figure 10.

Our results also lead to the conclusion that the thermostability of the capsid subunit is increased by about 10–15 °C as a result of RNA packaging. Both the subunit secondary structure and side-chain environments (particularly Trp, Tyr, and Phe) are affected. The 3.0-Å resolution crystal structure reveals at least 10 aromatic side chains (6 Phe, 3 Trp, 1 Tyr) near the RNA-binding pocket of the threefold vertex (Chen et al., 1989; Lomonossoff & Johnson, 1991). Trp-3170, Phe-3056, Phe-3171, Phe-3050, Phe-3127, and Phe-3146 are located near the protein C-domain–RNA interface, while Trp-3115, Trp-3156, Trp-2014, Phe-2106, and Tyr-2075 are located near the B-domain–RNA interface. Therefore, in addition to interactions proposed between positively charged side chains and RNA phosphates on the basis of the X-ray results, we propose RNA interactions with these aromatic side chains as a source of virion stabilization. Evidence for RNA interactions with subunit tryptophans has also been obtained from fluorescence studies of capsids and virions (J. Silva, personal communication).

Our comparisons of the Raman spectra of BPMV components in crystal and solution forms were conducted at one specific set of experimental conditions, viz., 8 °C, neutral pH, and moderate ionic strength of crystal mother liquor or aqueous solvent. For these specific conditions the spectrum of a given component is clearly *not* invariant to crystallization (Figure 8). Whether this would be true also over a wider range of experimental conditions remains to be determined. The precariousness of drawing general conclusions from these limited findings is accentuated by the fact that we observe the Raman spectrum of the middle component to be sensitive also to the concentration of KCl in solution. Therefore, we stress that the following observations apply only to the very limited conditions examined here: (i) Crystallization does not modify the secondary structures of subunits in either capsid or virions. (ii) However, crystallization causes minor structural adjustments in amino acid side chains, particularly for the empty capsid. (iii) Crystallization also perturbs nucleotides of the packaged RNA, and these perturbations are not identical for middle and bottom components. (iv) Most of the side-chain structural differences between crystalline and aqueous capsids are attenuated in the virions, possibly a result of specific RNA (or cofactor) binding which might act to "immobilize" side chains into configurations less sensitive to crystallization. (v) Since the RNA1 and RNA2 molecules are perturbed differently by their respective virion crystallizations, it seems likely that the balance of forces which leads to isomorphous crystallization of the two particles is not maintained in the corresponding solutions investigated here. This is perhaps not surprising, since the bottom component must package a 25% larger polyelectrolyte (i.e., RNA1) than the middle component (RNA2) utilizing an identical capsid. This imbalance may be overcome in the crystal by the roles of metal ions and polyamines. Our results suggest that these roles may be somewhat different in solution. This view is supported by the fact that many of the specific spectral differences between BPMV components in solution and crystalline states are qualitatively similar to the spectral differences between solutions of differing ionic strength (cf. Figures 8 and 9).

This study represents the first detailed spectroscopic analysis of a virus in crystalline and solution states. Many aspects of RNA structure, RNA–protein interaction, and thermostabilities of the RNA and protein components of BPMV are revealed by the Raman spectra. Future applications will focus on structural comparisons between the comoviruses and other ssRNA plant viruses and bacteriophages.

ACKNOWLEDGMENT

T.L. acknowledges graduate assistantship support from the UMKC School of Biological Sciences during the first year of this work and helpful discussions with Dr. James M. Benevides throughout the course of the project. We also thank Dr. Dennis Bamford, University of Helsinki, for the gift of purified dsRNA from bacteriophage ϕ6.

SUPPLEMENTARY MATERIAL AVAILABLE

Five figures showing Raman spectra of D_2O solutions of packaged and unpackaged BPMV RNA (Figure S1), Raman spectra of D_2O solutions of model base-paired structures (Figure S2), and temperature-dependent Raman spectra of

BPMV RNA (Figure S3), BPMV top component (Figure S4), and BPMV middle component (Figure S5) (7 pages). Ordering information is given on any current masthead page.

REFERENCES

Benevides, J. M., Weiss, M. A., & Thomas, G. J., Jr. (1991) *Biochemistry 30*, 5955–5963.

Chen, Z., Stauffacher, C., Li, Y., Schmidt, T., Wu, B., Kamer, G., Shanks, M., Lomonossoff, G., & Johnson, J. E. (1989) *Science 245*, 154–159.

Erfurth, S. C., Kiser, E. J., & Peticolas, W. L. (1972) *Proc. Natl. Acad. Sci. U.S.A. 69*, 938–941.

Harada, I., & Takeuchi, H. (1986) in *Spectroscopy of Biological Systems* (Clark, R. J. H., & Hester, R. E., Eds.) pp 156–162, Wiley, New York.

Johnson, J. E., Chen, Z., Li, Y., Schmidt, T., Stauffacher, C. V., Wery, J.-P., Hosur, M. V., & Sehnke, P. C. (1989) in *Synchrotron Radiation in Structural Biology* (Sweet, R. M., & Woodhead, A. D., Eds.) pp 141–159, Plenum Press, New York.

Lafleur, L., Rice, J., & Thomas, G. J., Jr. (1972) *Biopolymers 11*, 2423–2437.

Lamba, O. P., Wang, A. H.-J., & Thomas, G. J., Jr. (1989) *Biopolymers 28*, 667–678.

Li, T., Chen, Z., Johnson, J. E., & Thomas, G. J., Jr. (1990) *Biochemistry 29*, 5018–5026.

Li, Y., Thomas, G. J., Jr., Fuller, M., & King, J. (1981) *Prog. Clin. Biol. Res. 64*, 271–283.

Lippert, J. L., & Peticolas, W. L. (1971) *Proc. Natl. Acad. Sci. U.S.A. 68*, 1572–1576.

Lomonossoff, G. P., & Johnson, J. E. (1991) *Prog. Biophys. Mol. Biol. 55*, 107–137.

Lord, R. C., & Thomas, G. J., Jr. (1967) *Spectrochim. Acta 23A*, 2551–2591.

MacFarlane, S. A., Shanks, M., Davies, J. W., Zlotnick, A., & Lomonossoff, G. P. (1991) *Virology 183*, 405–409.

McKenna, R., Xia, D., Willingmann, P., Ilag, L. L., Krishnaswamy, S., Rossmann, M. G., Olson, N. H., Baker, T. S., & Incardona, N. L. (1992) *Nature 355*, 137–143.

Morikawa, K., Tsuboi, M., Takahashi, S., Kyogoku, Y., Mitsui, Y., Iitaka, Y., & Thomas, G. J., Jr. (1973) *Biopolymers 12*, 799–816.

Nishimura, Y., Tsuboi, M., Sato, T., & Aoki, K. (1986) *J. Mol. Struct. 146*, 123–153.

Prescott, B., Gamache, R., Livramento, J., & Thomas, G. J., Jr. (1974) *Biopolymers 13*, 1821–1845.

Prevelige, P. E., Jr., Thomas, D., King, J., Towse, S. A., & Thomas, G. J., Jr. (1990) *Biochemistry 29*, 5626–5633.

Semancik, J. S., & Bancroft, J. B. (1965) *Virology 27*, 476–483.

Small, E. W., & Peticolas, W. L. (1971) *Biopolymers 10*, 1377–1416.

Takeuchi, H., Kimura, Y., Koitabashi, I., & Harada, I. (1991) *J. Raman Spectrosc. 22*, 233–236.

Thomas, G. J., Jr. (1969) *Biopolymers 7*, 325–334.

Thomas, G. J., Jr. (1970) *Biochim. Biophys. Acta 213*, 417–423.

Thomas, G. J., Jr., & Barylski, J. R. (1970) *Appl. Spectrosc. 24*, 463–464.

Thomas, G. J., Jr., & Hartman, K. A. (1973) *Biochim. Biophys. Acta 312*, 311–322.

Thomas, G. J., & Agard, D. A. (1984) *Biophys. J. 46*, 763–768.

Thomas, G. J., Jr., Medeiros, G. C., & Hartman, K. A. (1971) *Biochem. Biophys. Res. Commun. 44*, 587–592.

Thomas, G. J., Jr., Benevides, J. M., & Prescott, B. (1986) *Biomol. Stereodyn. 4*, 227–254.

Tsao, J., Chapman, M. S., Agbandje, M., Keller, W., Smith, K., Wu, H., Luo, M., Smith, T. J., Rossmann, M. G., Compans, R. W., & Parrish, C. R. (1991) *Science 251*, 1456–1464.

Tsuboi, M., Takahashi, S., Muraishi, S., Kaijiura, T., & Nishimura, S. (1971) *Science 174*, 1142–1143.

Verduin, B. J. M., Prescott, B., & Thomas, G. J., Jr. (1984) *Biochemistry 23*, 4301–4308.

Virudachalam, R., Harrington, M., & Markley, J. (1985) *Virology 146*, 138–140.